Direct measurement of the entanglement of two superconducting qubits via state tomography

Matthias Steffen, M. Ansmann, Radoslaw C. Bialczak, N. Katz, Erik Lucero, R. McDermott, Matthew Neeley, E. M. Weig, A .N. Cleland, and John M. Martinis

Department of Physics and California Nanosystems Institute, University of California, Santa Barbara, California, USA

The laws of quantum physics provide intriguing possibilities for a tremendous increase in speed compared to classical computation[1]. Because this power is achieved through the controlled evolution of entangled quantum states, a clear demonstration of entanglement represents a key milestone towards the construction of a scalable quantum computer[2,3]. Although entanglement can be inferred from simple experiments, a direct demonstration is challenging because all of the DiVincenzo criteria[4] for quantum computation must be met simultaneously. Only subsets of these key requirements have been demonstrated previously for superconducting qubits[5-9]. Here, we demonstrate all of the DiVincenzo criteria simultaneously, thus taking a significant step forward towards placing superconducting qubits on the roadmap for scalable quantum computing. Specifically, capacitively-coupled Josephson phase qubits are used to create Bell states, which when measured using state tomography on both qubits show an entangled state with fidelity of up to 87%. Our results demonstrate a high degree of unitary control of the system, indicating that larger implementations are within reach.

Circuits made of superconductors and Josephson junctions are promising candidates for scalable quantum computation because of their compatibility with integrated-circuit fabrication technology[5-9]. The Josephson phase qubit stands apart from other

superconducting qubits because it does not require an optimal operating point. Coupling of phase qubits is thus straightforward, allowing for multiple control methods[10]. With recent improvements in coherence times and amplitudes[11], and the ability to measure both qubit states simultaneously[5], it is possible to use phase qubits to produce entangled states and measure them with high fidelity. We believe that demonstrations of quantum algorithms are also feasible.

A schematic of the phase qubit circuit is drawn in Fig. 1a. The Josephson junction (with critical current I_0) has a superconducting phase difference δ that serves as the quantum variable. When biased close to the critical current, the junction and its loop inductance L give a cubic potential that has qubit states $|0\rangle$ and $|1\rangle$, with an energy spacing that corresponds to a transition frequency $\omega_{10}/2\pi \sim 5$ GHz (see Fig. 1b). This frequency can be adjusted by ~30% via the bias current $I_\phi(t)$.

Single qubit logic operations, corresponding to rotations about the *x*, *y*, and *z*-axes of the Bloch sphere, are generated as follows. Rotations about the *z*-axis are produced from current pulses $I_Z(t)$ on the qubit bias line that adiabatically change the qubit frequency, leading to phase accumulation between the $|0\rangle$ and $|1\rangle$ states of the qubit[11]. Rotations about any axis in the *x*-*y* plane are produced by microwave pulses resonant with the qubit transition frequency. They selectively address only the qubit energy levels because transitions to higher lying energy levels are off-resonance due to the anharmonicity of the potential and the shaping of the pulses[12]. The phase of the microwave pulses defines the rotation axis in the *x*-*y* plane. The pulse duration and amplitude control the rotation angle.

The qubit state is measured by applying a strong pulse to I_Z so that only the $|1\rangle$ state tunnels out of the cubic well (see Fig. 1c). Once tunnelled, the state quickly decays into an external ground state that can be easily distinguished from the $|0\rangle$ state by an on-chip SQUID amplifier.

Two separate phase qubits are coupled with a fixed capacitor[5], as sketched in Fig. 1d. With the qubits labelled *A* and *B*, the coupling Hamiltonian is $H_{\rm int} = (S/2)(|01\rangle\langle 10| + |10\rangle\langle 01|)$, where $|01\rangle = |0\rangle_A \otimes |1\rangle_B$. The coupling strength $S = (C_x / C)\hbar\omega_{10}$ is proportional to the coupling capacitance $C_x \approx 3$ fF, and $C \approx 1.3$ pF is the value of the shunting capacitor (see Methods section). The two qubits may easily be brought into resonance, even though they are not identical, because each can be tuned over a large frequency range. On resonance, the interaction produces an oscillation with frequency S/h between the states $|01\rangle$ and $i|10\rangle$. For an interaction time of $h/4S$ the coupling produces the $\sqrt{iSWAP}$ gate: this gate, together with single qubit gates, is universal[13]. The coupling also manifests itself as an avoided level crossing of strength S/h in the spectroscopy of the individual qubits[14].

The performance of each qubit can be determined separately by strongly detuning the two qubits relative to S/h so that they behave independently. A standard set of experiments, including Rabi and Ramsey oscillations, spin echo sequences and inversion recovery experiments, give an energy relaxation time $T_1 = 130$ ns and a dephasing time $T_2^* = 80$ ns for each qubit. These results are consistent with measured values of an uncoupled sample[11], indicating no additional loss due to the second qubit. The measurement fidelities, defined as the probability of correctly identifying the state $|0\rangle$ ($|1\rangle$), are $F_0 = 0.95$ ($F_1 = 0.85$).

We next tune both qubits to $\omega_{10}/2\pi = 5.1$ GHz and determine the splitting $S/h = 10$ MHz by qubit spectroscopy. The time dynamics of the coupling is verified by initializing the qubits to the $|00\rangle$ state and applying to qubit *B* a 180° rotation about the *x* axis (180_x pulse) of duration 10ns. This pulse is sufficiently long to avoid unwanted transitions to other energy levels, but short on the time scale of the coupling. The resulting state $|01\rangle$ is not an eigenstate of the coupling Hamiltonian, and thus evolves in time according to $|\psi(t)\rangle = \cos(St/2\hbar)|01\rangle + i\sin(St/2\hbar)|10\rangle$. After a variable free-

evolution time t_{free}, we simultaneously measure the state of the two qubits. Repeating the experiment approximately 1,000 times, we determine the occupation probabilities P_{00}, P_{01}, P_{10}, and P_{11}. This sequence of operations is depicted in Fig. 2a, and the measured probabilities are plotted in Fig. 2b.

The occupation probabilities P_{01} and P_{10} oscillate out of phase with a period of 100 ns, consistent with the spectroscopic measurements. The amplitude and decay of the data is also compatible with the separately measured lifetimes and measurement fidelities of the single qubits. Compared to earlier experiments[5], the amplitude of the measured oscillations is significantly larger because of improvements in single qubit fidelities. We note that the oscillations persist longer than the dephasing time $T_2^* = 80$ ns because the period of the coupled qubit oscillations shown in Fig. 2 is, to first order, insensitive to the detuning of the qubits. For these states, this represents "self-refocusing" of low-frequency noise, or equivalently, a degeneracy point that is also tunable.

Although this data is consistent with the production of an entangled state at time $t_{free} = 25$ ns, a more stringent test includes performing coherent single qubit operations on this entangled state to verify the predicted unitary evolution of the system. After the application of a180_x pulse on qubit B and a free evolution time of $t_{free} = 25$ ns, the system is in the entangled state $|\psi_1\rangle = (|01\rangle - i|10\rangle)/\sqrt{2}$. By then applying a 90_z pulse on qubit B, we create the Bell state $|\psi_2\rangle = (|01\rangle - |10\rangle)/\sqrt{2}$. Because $|\psi_2\rangle$ is an eigenstate of the coupling Hamiltonian, it should not evolve with time. Implementation of this sequence of operations is complicated by the coupling interaction that occurs during the single qubit operations. Compared with the coupling interaction time $t_{free} = 25$ ns, the duration of the single qubit gates 180_x and 90_z are 10 ns and 4 ns, respectively, and are thus not negligible. The excess coupled interaction during the single qubit gates can be significantly compensated by reducing the free evolution time[15] to $t_{free} = 16$ ns, which we checked numerically. Upon executing this sequence of

operations, we verify that indeed P_{01} and P_{10} no longer oscillate as a function of t_{free}, as shown in Fig. 2c.

This observed behaviour, however, could also be attributed to the destruction of coherence between the states $|01\rangle$ and $|10\rangle$ caused by the application of the 90_z pulse. To check this possibility, we instead apply a 180_z pulse on qubit *B* when the system is in the state $|\psi_1\rangle$, creating the state $|\psi_3\rangle = (|01\rangle + i|10\rangle)/\sqrt{2}$. Because $|\psi_3\rangle$ is equivalent to $|\psi_1\rangle$ but delayed by $t_{free} = 50$ ns, a reversal of the oscillations is predicted for this experiment. This prediction is verified by the data in Fig. 2d, and provides further evidence of an entangled state.

A full and unambiguous test of entanglement comes from state tomography[2,3,16], which involves the measurement of the quantum state in all nine combinations of three measurement bases (*x*, -*y*, and *z*) for each qubit. Each measurement gives three unique probabilities (e.g. P_{01}, P_{10}, P_{11}) for a total of 27 numbers, which are used to compute the 15 independent parameters of the unknown density matrix ρ via a least squares fit[16]. The measurement basis change from *z* to *x* (-*y*) arises from applying a 90_y (90_x) microwave pulse before measurement[11].

After calibrating the phase of the microwave pulses for the two qubits (see Methods section) we perform state tomography on $|\psi_1\rangle$, as indicated by the sequence of operations in Fig. 3a. As in the previous experiment, we reduced the duration of the free evolution to compensate for coupled qubit interaction during the initial 180_x pulse and the tomography pulses. After executing all nine tomography sequences and measuring the resulting occupation probabilities, we compute the density matrix ρ_{exp}. The real and imaginary parts of the reconstructed density matrix ρ_{exp} are shown in Fig 3b. The imaginary off-diagonal elements $|01\rangle\langle 10|$ and $|10\rangle\langle 01|$ have nearly the same magnitude as the diagonal components $|01\rangle\langle 01|$ and $|10\rangle\langle 10|$, clearly revealing a coherent superposition of the states $|01\rangle$ and $|10\rangle$. This measurement unambiguously verifies

that the two qubits are indeed entangled. Compared to the ideally expected density matrix $\sigma = |\psi_1\rangle\langle\psi_1|$, we compute the fidelity of the reconstructed quantum state and find $F_{\exp} = tr\sqrt{\sigma^{1/2}\rho_{\exp}\sigma^{1/2}} = 0.75$.

To identify the sources of fidelity loss, we first correct for measurement error. Based on the measurement fidelities discussed earlier, we renormalize the measured occupation probabilities and calculate the intrinsic occupation probabilities (see Methods). From this we compute a density matrix corrected for measurement $\rho_{\exp,M}$ (see Fig. 3c) that gives an improved fidelity $F_{\exp,M} = tr\sqrt{\sigma^{1/2}\rho_{\exp,M}\sigma^{1/2}} = 0.87$. We attribute most of the remaining fidelity loss to single-qubit decoherence. By modelling decoherence effects[15] using the measured relaxation times, we obtain an expected density matrix ρ_{th} that gives a fidelity $F_{th} = tr\sqrt{\sigma^{1/2}\rho_{th}\sigma^{1/2}} = 0.89$, which is close to the normalized measured value[17]. The fact that our error is dominated by decoherence indicates good unitary control of our system and thus suggests that improvements in coherence times will directly translate to enhanced gate fidelities. Dramatic increases in coherence should be possible based on straightforward improvements in the dielectric material of the shunting capacitor[11,19].

In conclusion, we have performed experiments on coupled phase qubits and verified by state tomography the creation of an entangled Bell state with 87% fidelity. Given that most of the loss in fidelity can be attributed to decoherence, we believe that more complex implementations are well within reach with only modest improvements in qubit coherence times.

Methods

Phase Qubit The design concepts behind this phase qubit have been discussed previously[11]. A ~1 μm^2 area tunnel junction was shunted by a capacitor to reduce the effective density of two-level defects of the tunnel barrier, improving the coherence

amplitude of the qubit[11]. Amorphous silicon nitride was used for the dielectric material of the shunting capacitor: its loss tangent is consistent with the measured energy relaxation time. Parameters of the circuit are $C \sim 1.3$ pF, $L \sim 850$ pH, and $I_0 \sim 1.1$ μA.

The two phase qubits are coupled via a *3* fF interdigitated capacitor, giving an interaction strength of $S/h = 10$ MHz. Measurement crosstalk[5] between the qubits is expected to be insignificant because of the small interaction strength, as confirmed by measurements.

Microwaves The microwave pulses are generated using an IQ mixer. Phase and amplitude control is achieved by adding the signal of the two quadrature components (I and Q) of a continuous wave microwave signal, with separate amplitude control for each channel[11]. One microwave source and two IQ mixers were used to achieve phase and amplitude control of the microwave pulses for both qubits.

State Tomography Implementing state tomography requires calibration of the phase difference between the microwave pulses reaching the qubits, as the rotation axis depends on phase. Even if the same microwave pulse is generated by both mixers, the actual phase observed by the qubits differs because the microwave lines have slightly different lengths. Calibration of this phase offset is done in a separate experiment by simultaneously applying a 90_x pulse on qubit *A* and a 90_θ pulse on qubit *B*, where θ is an adjustable microwave phase angle. A plot of the occupation probabilities versus free evolution time gives oscillations whose amplitude depends on the phase angle θ. The oscillation amplitudes of P_{01} and P_{10} are maximized (minimized) whenever the relative phase between the $|01\rangle$ and $|10\rangle$ states is 90 (0) degrees. When the oscillation amplitude is maximized *and* P_{10} peaks first, θ corresponds to a y-rotation for the second qubit and serves as our calibration.

The intrinsic occupation probabilities P_i for the two qubits can be inferred from the measured probabilities $P_m = (P_{00}, P_{01}, P_{10}, P_{11})^T$ and the measurement fidelities $F_0 = 0.95$ and $F_1 = 0.85$ (see text). The intrinsic occupation probabilities are computed as $P_i = F^{-1} P_m$ where

$$F = \begin{pmatrix} F_0^2 & F_0(1-F_1) & F_0(1-F_1) & (1-F_1)^2 \\ (1-F_0)F_0 & F_0F_1 & (1-F_0)(1-F_1) & (1-F_1)F_1 \\ (1-F_0)F_0 & (1-F_0)(1-F_1) & F_0F_1 & (1-F_1)F_1 \\ (1-F_0)^2 & (1-F_0)F_1 & (1-F_0)F_1 & F_1^2 \end{pmatrix}$$

We verified that none of the inferred intrinsic probabilities were negative. The measured probabilities were computed from 20,000 executions of the same experiment.

1. Nielsen, M. A. & Chuang, I. L. *Quantum computation and quantum information*. (Cambridge University Press, Cambridge, 2000)
2. Häffner, H. *et al.* Scalable multiparticle entanglement of trapped ions. *Nature* **438**, 643–646 (2005)
3. Leibfried, D. *et al.* Creation of a six-atom 'Schrödinger cat' state. *Nature* **438**, 639–642 (2005)
4. DiVincenzo, D. P. The physical implementation of quantum computers. *Fortschr. Physik* **48,** 771–783 (2000).
5. McDermott, R. *et al.* Simultaneous state measurement of coupled Josephson phase qubits. *Science* **307**, 1299–1302 (2005)
6. Yamamoto, T. *et al.* Demonstration of conditional gate operation using superconducting charge qubits. *Nature* **425**, 941–944 (2003)
7. Vion, D. *et al.* Manipulating the quantum state of an electrical circuit. *Science* **296**, 886–889 (2002)

8. Chiorescu, I. *et al.* Coherent quantum dynamics of a superconducting flux qubit. *Science* **299**, 1869–1871 (2003)

9. Wallraff, A. *et al*. Approaching unit visibility for control of a superconducting qubit with dispersive readout. *Phys. Rev. Lett.* **95**, 060501 (2005)

10. Geller, M. *et al.* in preparation

11. Steffen, M. *et al*. State tomography of a capacitively shunted phase qubit with high fidelity. *Submitted to Phys. Rev. Lett.* (2006)

12. Steffen, M., Martins J.M. & Chuang, I.L. Accurate control of Josephson phase qubits. *Phys. Rev. B.* **68**, 224518 (2003)

13. Schuch, N. & Siewert, J. Natural two-qubit gate for quantum computation using the XY interaction. *Phys. Rev. A.* **67**, 032301 (2003)

14. Berkeley, A.J. *et al.* Entangled macroscopic quantum states in two superconducting qubits. *Science* **300**, 1548 – 1550 (2003)

15. Vandersypen, L.M.K. *et al.* Experimental realization of Shor's quantum factoring algorithm using nuclear magnetic resonance. *Nature* **414**, 883 – 887 (2001)

16. Vandersypen, L. M. K. *et al*. Implementation of three-quantum-bit search algorithm. *Appl. Phys. Lett.* **76,** 646–648 (2000).

17. A more stringent measure that quantifies the amount of entanglement, even for mixed states, is the entanglement fidelity[18] $E(\rho)$. We find $E(\rho_{\exp,M}) = 0.42$ compared with $E(\rho_{th}) = 0.61$.

18. Wootters W. K. Entanglement of formation and concurrence. *Quant. Inf. Comp.* **1**, 27 – 44, 2001

19. Martinis, J.M. *et al.* Decoherence in Josephson qubits from dielectric loss. *Phys. Rev. Lett.* **95**, 210503 (2005)

Acknowledgment We acknowledge Steve Waltman and NIST for support in building the microwave electronics. Devices were made at the UCSB and Cornell Nanofabrication Facilities, a part of the NSF funded NNIN network. N. K. acknowledges support of the Rothschild fellowship. This work was supported by ARDA under grant W911NF-04-1-0204 and NSF under grant CCF-0507227.

Correspondence and requests for materials should be addressed to J.M.M. (martinis@physics.ucsb.edu).

Figure 1 Qubit circuit and experimental operation. (a) Circuit schematic for a single Josephson phase qubit, where the X symbol represents the Josephson junction. The measurement is implemented with a broadband 50 Ω transmission line with cold attenuators that is connected to the flux bias line with a bias tee. (b) Operation mode of the qubit showing the potential energy U versus junction phase δ. The qubit is formed from the two lowest eigenstates $|0\rangle$ and $|1\rangle$, with a transition frequency $\omega_{10}(I_{dc})/2\pi$ =5.1 GHz that can be adjusted by varying the bias I_ϕ. (c) Measurement mode of the qubit. During the measurement pulse, the energy barrier ΔU is lowered to increase the tunnelling probability of $|1\rangle$. (d) An interdigitated capacitor with $C_x \sim 3$ fF couples the qubits, giving rise to an interaction strength of magnitude $S/h = 10$ MHz.

Figure 2 Coherent operations on coupled phase qubits. (a) Sequence of operations. A 10ns long, 180_x pulse is applied to qubit B, populating the $|01\rangle$ state. Following a free evolution period t_{free} in which the qubits interact, the state occupation probabilities are measured using 10 ns current pulses that induce selective tunnelling of the $|1\rangle$ state. For data in (c) and [(d)], a 90_z [180_z] pulse is applied to qubit B after 16 ns. (b) Plot of measurement probabilities of the states $|01\rangle$, $|10\rangle$, and $|11\rangle$ as a function of t_{free}. Note that $P_{00} = 1 - P_{01} - P_{10} - P_{11}$. The solid lines are the results of simulations using known

measurement fidelities, relaxation times, and microwave crosstalk. (c) Plot of measurement probabilities for a sequence that creates the eigenstate $|\psi_2\rangle = (|01\rangle - |10\rangle)/\sqrt{2}$ of the coupling Hamiltonian. After the eigenstate is formed by the 90_z pulse, it ceases to evolve with time. (d) As in (c), but with an 180_z pulse. Here, the phase of the oscillation changes by 180 degrees.

Figure 3 State tomography of entangled quits. (a) Sequence of operations. A 180_x pulse is first applied to qubit B, followed by a free evolution period of about 16 ns, creating the entangled state $|\psi_1\rangle = (|01\rangle - i|10\rangle)/\sqrt{2}$. State tomography is then performed using 4 ns single qubit rotations. (b) Reconstructed density matrix ρ_{exp} (real and imaginary parts) using the directly measured occupation probabilities. (c) Reconstructed density matrix $\rho_{\text{exp},M}$ after correcting the state occupation probabilities based on the single qubit measurement fidelities.

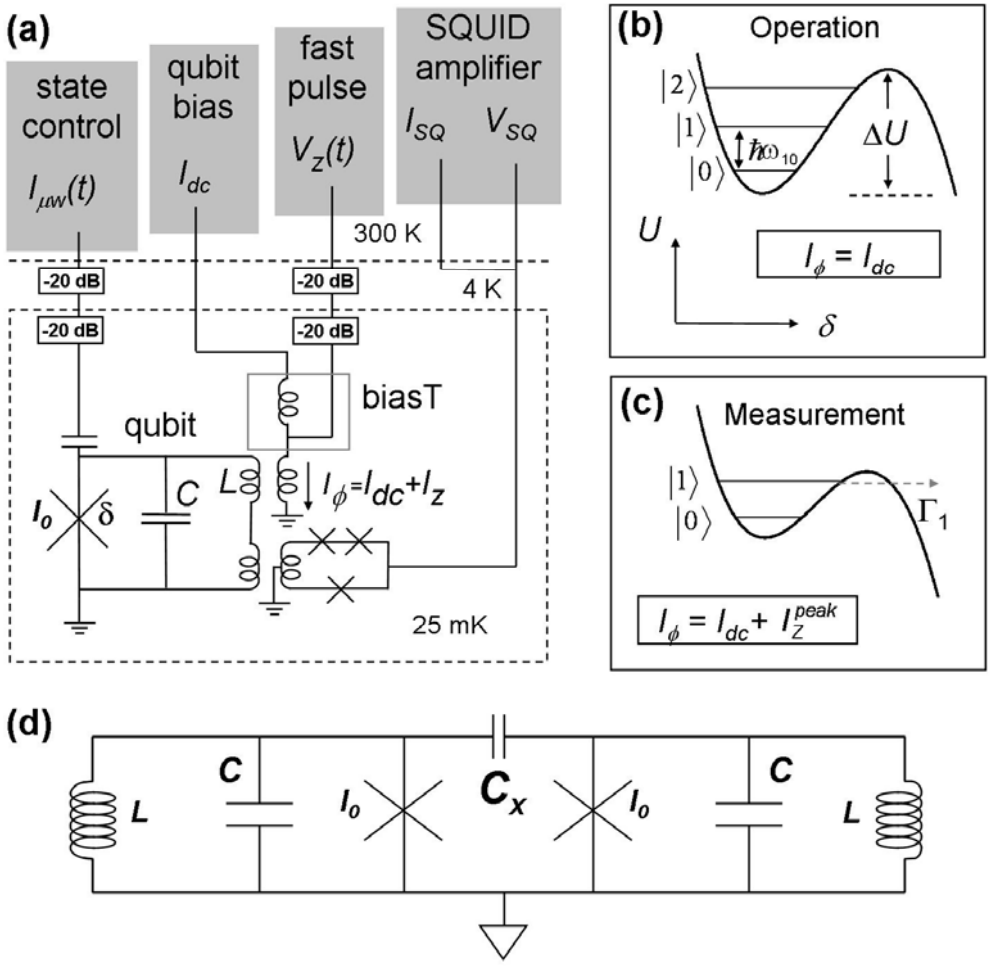
(a)
state control
$I_{\mu w}(t)$
qubit bias
I_{dc}
fast pulse
$V_Z(t)$
SQUID amplifier
I_{SQ}
V_{SQ}
300 K
4 K
-20 dB
-20 dB
-20 dB
-20 dB
qubit
biasT
I_o
δ
C
L
$I_\phi = I_{dc} + I_Z$
25 mK
(b)
Operation
$|2\rangle$
$|1\rangle$
$|0\rangle$
$\hbar\omega_{10}$
ΔU
U
δ
$I_\phi = I_{dc}$
(c)
Measurement
$|1\rangle$
$|0\rangle$
Γ_1
$I_\phi = I_{dc} + I_Z^{peak}$
(d)
L
C
I_o
C_x
I_o
C
L

FIGURE 1

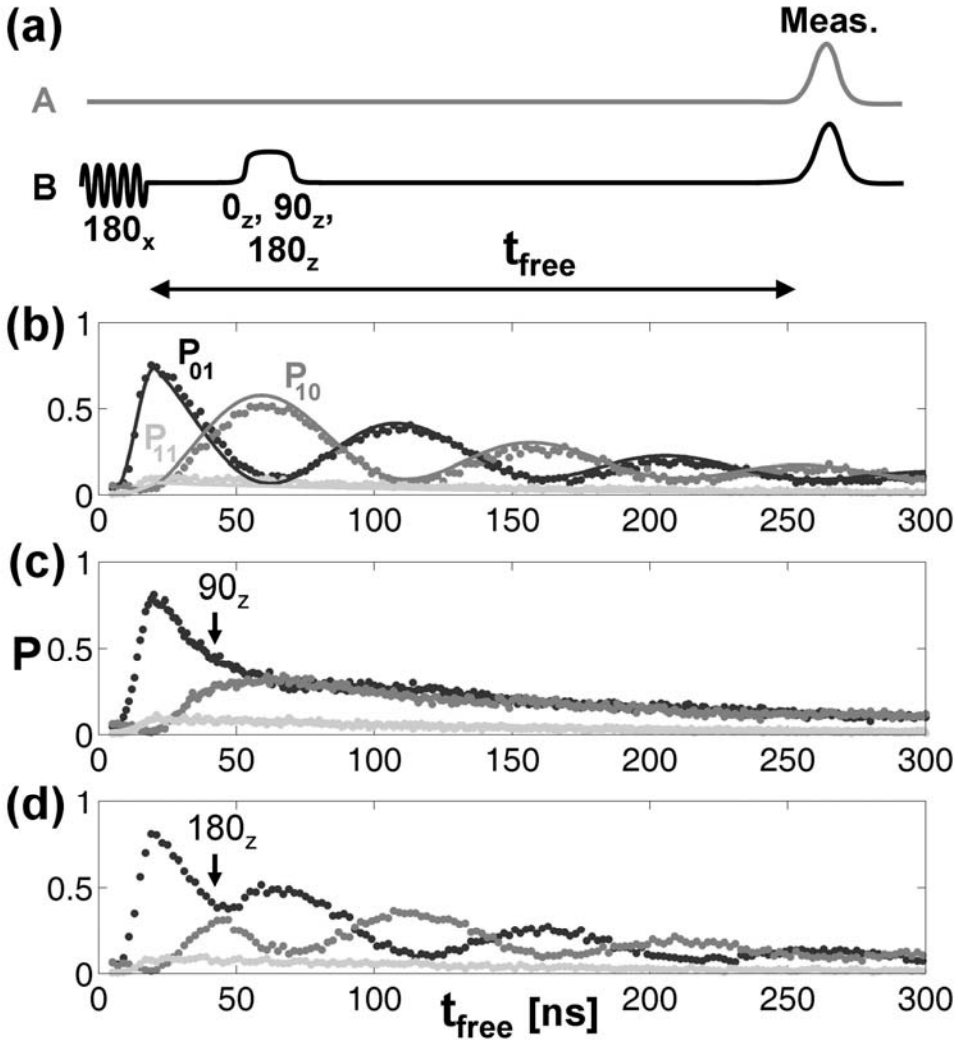
(a)
Meas.
A
B
180x
0z, 90z,
180z
tfree
(b)
P01
P10
P11
(c)
90z
P
(d)
180z
tfree [ns]

FIGURE 2

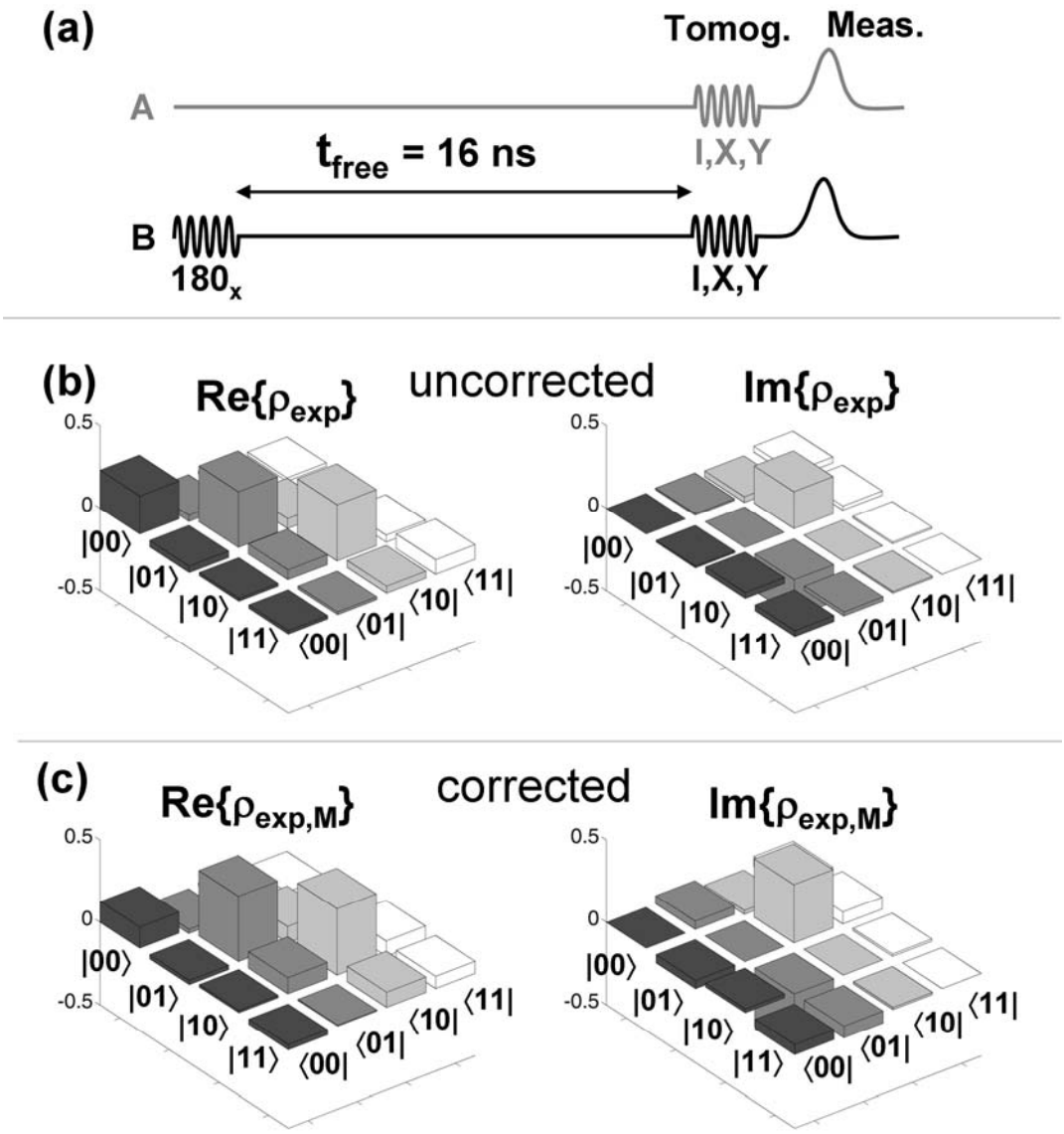
(a)
Tomog.
Meas.
A
t_{free} = 16 ns
I,X,Y
B
180_x
I,X,Y
(b)
$Re\{\rho_{exp}\}$
uncorrected
$Im\{\rho_{exp}\}$
0.5
0
-0.5
|00⟩
|01⟩
|10⟩
|11⟩
⟨00|
⟨01|
⟨10|
⟨11|
(c)
$Re\{\rho_{exp,M}\}$
corrected
$Im\{\rho_{exp,M}\}$

FIGURE 3